J Neurophysiol 102: 532–545, 2009.
First published May 20, 2009; doi:10.1152/jn.00305.2009.

Sparse but Selective and Potent Synaptic Transmission From the Globus Pallidus to the Subthalamic Nucleus

Jérôme Baufreton,[1,2] Erin Kirkham,[1] Jeremy F. Atherton,[1] Ariane Menard,[1] Peter J. Magill,[3] J. Paul Bolam,[3] and Mark D. Bevan[1,3]

[1]*Department of Physiology, Northwestern University, Chicago Illinois;* [2]*Université de Bordeaux 2; Centre National de la Recherche Scientifique, Unité Mixte de Recherche 5227, Bordeaux Cedex, France; and* [3]*Department of Pharmacology, Medical Research Council Anatomical Neuropharmacology Unit, Oxford University, Oxford, United Kingdom*

Submitted 6 April 2009; accepted in final form 11 May 2009

Baufreton J, Kirkham E, Atherton JF, Menard A, Magill PJ, Bolam JP, Bevan MD. Sparse but selective and potent synaptic transmission from the globus pallidus to the subthalamic nucleus. *J Neurophysiol* 102: 532–545, 2009. First published May 20, 2009; doi:10.1152/jn.00305.2009. The reciprocally connected GABAergic globus pallidus (GP)-glutamatergic subthalamic nucleus (STN) network is critical for voluntary movement and an important site of dysfunction in movement disorders such as Parkinson's disease. Although the GP is a key determinant of STN activity, correlated GP-STN activity is rare under normal conditions. Here we define fundamental features of the GP-STN connection that contribute to poorly correlated GP-STN activity. Juxtacellular labeling of single GP neurons in vivo and stereological estimation of the total number of GABAergic GP-STN synapses suggest that the GP-STN connection is surprisingly sparse: single GP neurons maximally contact only 2% of STN neurons and single STN neurons maximally receive input from 2% of GP neurons. However, GP-STN connectivity may be considerably more selective than even these estimates imply. Light and electron microscopic analyses revealed that single GP axons give rise to sparsely distributed terminal clusters, many of which correspond to multiple synapses with individual STN neurons. Application of the minimal stimulation technique in brain slices confirmed that STN neurons receive multisynaptic unitary inputs and that these inputs largely arise from different sets of GABAergic axons. Finally, the dynamic-clamp technique was applied to quantify the impact of GP-STN inputs on STN activity. Small fractions of GP-STN input were sufficiently powerful to inhibit and synchronize the autonomous activity of STN neurons. Together these data are consistent with the conclusion that the rarity of correlated GP-STN activity in vivo is due to the sparsity and selectivity, rather than the potency, of GP-STN synaptic connections.

INTRODUCTION

The reciprocally connected GABAergic globus pallidus (GP) and glutamatergic subthalamic nucleus (STN) form a key network within the basal ganglia, a group of subcortical brain nuclei that are critical for voluntary movement and the principal site of pathology and dysfunction in Parkinson's disease (PD) (Albin et al. 1989; DeLong 1990; Graybiel et al. 1994; Hornykiewicz 2006; Israel and Bergman 2008). Although the GP and STN are reciprocally connected (Shink et al. 1996; Smith et al. 1990) and GP and STN neurons powerfully pattern each other's activity (Baufreton et al. 2005; Bevan et al. 2002; Hallworth and Bevan 2005; Hanson et al. 2004; Maurice et al. 1999; Nambu et al. 2000), temporally correlated firing within and between the GP and STN is detected rarely at rest or during normal motor function (Mallet et al. 2008a; Raz et al. 2000; Urbain et al. 2000; Wichmann et al. 1994). In contrast, widespread, correlated GP-STN activity emerges in association with the motor symptoms of PD (Bergman et al. 1994; Levy et al. 2000; Moran et al. 2008; Raz et al. 2000). The detrimental nature of hyper-synchronous activity is further evidenced by the fact that normalization of GP and STN activity through administration of L-DOPA or high-frequency electrical stimulation of the STN profoundly ameliorates the motor symptoms of PD (Benabid 2003; Brown et al. 2001; Hamani et al. 2006; Levy et al. 2001). It is therefore imperative to determine the principles that maintain decorrelated GP-STN activity under normal conditions. To address this issue, a series of anatomical and electrophysiological studies were carried out in rats, a species that exhibits normal and pathological patterns of GP and STN activity that are analogous to those reported in human and non-human primates (Magill et al. 2000, 2001; Mallet et al. 2008a,b; Urbain et al. 2000).

The anatomical substrates through which GABAergic GP neurons influence the STN, including the number and spatial distribution of target neurons and the placement of synapses are likely to be major determinants of the level of correlation between the GP and STN (Terman et al. 2002). Indeed studies of cortex, which normally exhibits greater synchronization than GP and STN, suggest that GABAergic inputs are essential for correlated activity (Csicsvari et al. 2003; Fuchs et al. 2007; Hasenstaub et al. 2005). By innervating a high proportion of neighboring pyramidal neurons and forming multiple synaptic connections close to the site of action potential initiation, individual GABAergic interneurons potently synchronize cortical activity (Cobb et al. 1995; Halasy et al. 1996; Kraushaar and Jonas 2000). Our first objective was therefore to determine whether the structural organization of the GABAergic GP-STN connection contributes to decorrelated STN activity by mapping the number and distribution of GP-STN terminals that arise from individual GP neurons, stereological estimation of the total number of GABAergic GP-STN synapses, and correlated light and electron microscopy of individual GP-STN axons.

Our second objective was to determine whether inputs arising from single or small numbers of GP neurons decorrelate or correlate the activity of STN neurons. This objective was addressed in brain slices first through minimal stimulation of

Address for reprint requests and other correspondence: M. D. Bevan, Dept. of Physiology, Northwestern University, 303 E. Chicago Ave, Chicago, Il 60611 (E-mail: m-bevan@northwestern.edu); or J. Baufreton, Université de Bordeaux, CNRS UMR 5227, 146 Rue Léo Saignat, 33076 Bordeaux Cedex, France (E-mail: jerome.baufreton@u-bordeaux2.fr).

GP-STN axons during recordings of neighboring STN neurons and second, through the injection of a range of synthetic synaptic conductances (Robinson and Kawai 1993; Sharp et al. 1993), the magnitude and kinetics of which were informed by the estimates described above and measurements of miniature and evoked GP-STN transmission.

METHODS

All procedures involving the use of experimental animals were carried out in accordance with the American Physiological Society, Northwestern University's Institutional Animal Care and Use Committee and the Animals (Scientific Procedures) Act 1986 (United Kingdom).

Number and targets of GP-STN terminals arising from single GP neurons

Labeling of single neurons with neurobiotin (Vector Laboratories; Burlingame, CA) was carried out in 10 adult rats (6 Wistar and 4 Sprague-Dawley) that were deeply anesthetized with ketamine (100 mg/kg ip; Ketaset, Willows Francis, Crawley, UK) and xylazine (10 mg/kg ip; Rompun, Bayer, Germany) using the juxtacellular technique as described previously (Bevan et al. 1998; Magill et al. 2000; Pinault 1996). Ten to 14 h after labeling, animals under the same anesthetic were perfused with 20–50 ml phosphate buffered saline, 300 ml 0.3% glutaraldehyde and 3% paraformaldehyde in 0.1 M phosphate buffer (PB) and 200 ml of 3% paraformaldehyde in PB. Sagittal sections (50–70 μm) of brain were prepared with a vibratome (VT1000s, Leica Microsystems, Nussloch, Germany) and then rendered permeable through 0.3% Triton X-100 (light microscopy) or freeze–thawing in cooled isopentane and liquid nitrogen (electron microscopy). Neurobiotin was revealed by incubations in avidin–biotin peroxidase complex (1:100, Vector Laboratories) and then hydrogen peroxide and diaminobenzidine (DAB, Sigma-Aldrich, St Louis, MO) in the presence or absence of Ni^{2+}. Sections were then processed for light microscopy only or correlated light and electron microscopy as described previously (Bevan et al. 1998). Digital images of labeled GP neurons were acquired using a microscope equipped with a CCD camera (Axioskop/Axiocam, Zeiss, Oberkochen, Germany).

The boundaries of the GP and STN and the location of labeled GP neurons and GP-STN axon terminals were charted with a microscope (DM LB, Leica Microsystems) equipped with a Neurolucida reconstruction system (MicroBrightfield, Williston, VT). In material that was not postfixed with OsO_4 there was shrinkage in the *z* axis but not the *y* or *x* axes. *Z* coordinates were therefore corrected for shrinkage (Zheng and Wilson 2002). Shrinkage was negligible in sections that were postfixed with OsO_4, as described previously (Kincaid et al. 1998). The coordinates encoding the boundaries of terminal fields and positions of terminals were plotted using Igor Pro 6 (Wavemetrics; Lake Oswego, OR). For comparison with GP-STN terminal distributions, fields of randomly distributed terminals were simulated using a pseudorandom number generator. Simulated terminals were then subjected to a "crossings test," an application of Jordan Curve Theorem (Haines 1994; Press et al. 1992), to ensure that they resided within the boundaries of GP-STN fields.

Several clusters of labeled GP-STN terminals were re-sectioned using an ultramicrotome (UCT, Leica Microsystems). Serial ultrathin sections through GP-STN terminals were then mounted on pioloform-coated slot grids, stained with lead citrate and examined and photographed using an electron microscope (Jeol 1200, Jeol USA, Peabody, MA) (Bevan et al. 1998).

Stereological analysis of the GP-STN connection

Two adult Sprague-Dawley and two Wistar rats were perfused with fixative, as described in the preceding text except that 300 ml of 5% glutaraldehyde was employed. Serial 70-μm sagittal sections of the STN were then cut and prepared for light and electron microscopy. The boundaries of the STN on each section were then charted with Neurolucida. The volume of the STN in each hemisphere was estimated using the Cavalieri method. The volume of the STN in each section was first calculated by multiplying the area of the STN by the thickness of each respective section. The total volume of the STN in each hemisphere was then calculated by summing the volume of STN in each section (West 1999).

Serial ultrathin sections from four regions of the STN were collected and processed for the detection of GABA-immunoreactivity using the postembedding immunogold technique (Bevan et al. 1995). Grids were washed in 0.05 M Tris buffer containing 0.9% NaCl and 0.01% Triton X-100 and then incubated sequentially in 1:25,000 rabbit anti-GABA antiserum (A2052; Sigma) and 1:100 15 nm gold-conjugated goat anti-rabbit IgG (British BioCell, Cardiff, UK). The grids were then washed and prepared for viewing in the electron microscope. Adjacent pairs of ultrathin sections of similar thickness (50–70 nm) (Small 1968) were examined at $\times$15,000–20,000 using the "dissector" technique to determine the density of GP-STN synapses (West 1999). Each pair of electron micrographs represents two "dissectors" with micrograph 1 acting as the "reference" section and micrograph 2 acting as the "look-up" section and vice versa. GABA-immunoreactive structures by definition possessed a density of immunogold particles that was more than five times the immunoreactivity of glutamatergic STN neurons. Synapses were counted if they were GABA-immunoreactive and symmetrical and present in the reference but not the look-up section. The density of GABAergic symmetrical (putative GP-STN) synapses was determined by the total number of "counted" synapses divided by the total sample volume (sample volume per reference section = sample area $\times$ reference section thickness). The total number of GABAergic symmetrical (putative GP-STN) synapses in the STN was then estimated by multiplying the density of synapses by the volume of the STN as estimated in the preceding text.

Physiological properties of the GP-STN connection

Sagittal (300 μm thick) brain slices through the STN were prepared from 18- to 25-day-old Sprague Dawley rats as described previously (Baufreton and Bevan 2008). Individual slices were recorded in a chamber that was perfused with media that was heated to 37°C, equilibrated with 95% O_2-5% CO_2, and contained (in mM) 126 NaCl, 3 KCl, 1.25 $NaH_2PO_4.H_2O$, 1.6 $CaCl_2.2H_2O$, 1.5 $MgSO_4.7H_2O$, 10 glucose, and 26 $NaHCO_3$. Neurons were visualized under infrared gradient contrast video microscopy (Infrapatch workstation; Luigs and Neumann, Ratingen, Germany). Somatic patch clamp recordings were made using 2–5 MΩ pipettes. $GABA_A$ receptor-mediated inhibitory postsynaptic currents (IPSCs) were evoked by bipolar minimal electrical stimulation of internal capsular fibers rostral to the STN (10–500 μA; A360 stimulus isolator; World Precision Instruments, Sarasota, FL). This region contains the main descending axons of GP neurons and is rostral to point where GP axons branch and give rise to collaterals in the STN (Bevan et al. 1998; Kita and Kitai 1994). The poles of stimulation were selected from a 20-electrode matrix (Frederick Haer, Bowdoinham, ME). For the recording of evoked IPSCs or miniature IPSCs (mIPSCs, in the presence of 1 μM TTX) at -60 mV, pipettes were filled with (in mM) 135 CsCl, 3.6 NaCl, 1 $MgCl_2$, 10 HEPES, 10 QX-314, 0.1 Na_4EGTA, 0.4 Na_3GTP, and 2 $Mg_{1.5}ATP$. $GABA_A$ receptor-mediated IPSCs were isolated by bath application of 1 μM (2S)-3-[[(1S)-1-(3,4-dichlorophenyl)ethyl]amino 2hydroxypropyl](phenylmethyl)phosphinic acid (CGP55845), 50 μM D-(–)-2-amino-5-phosphonopentanoic acid (APV), and 20 μM 6,7-dinitroquinoxaline-2,3-dione (DNQX) to block $GABA_B$, *N*-methyl-D-aspartate (NMDA), and AMPA-kainate receptors, respectively. In several cases, a $GABA_A$ receptor antagonist (20 μM GABAzine) was bath-

applied to confirm that IPSCs were indeed mediated by $GABA_A$ receptors.

For the injection of synthetic synaptic conductances in current-clamp mode, pipettes were filled with (in mM) 135 KMeSO4, 3.8 NaCl, 1 $MgCl_2$, 10 HEPES, 0.1 Na_4EGTA, 0.4 Na_3GTP, and 2 $Mg_{1.5}ATP$. For perforated-patch recordings, the pipette solution also contained gramicidin D (15 μg/ml; Sigma). Single synthetic inhibitory postsynaptic potentials (IPSPs) were generated using a SM-1 conductance injection amplifier (Cambridge Conductance, Cambridge, UK), as described previously (Baufreton and Bevan 2008; Baufreton et al. 2005). Spontaneous synaptic transmission was blocked, as in the preceding text. Electrophysiological data were recorded using a Multiclamp 700B amplifier controlled by Clampex 10 (Molecular Devices, Union City, CA), digitized at 10–50 kHz and low-pass filtered at 2–10 kHz. Junction potentials were corrected, as described previously (Baufreton and Bevan 2008).

IPSCs were detected and analyzed using miniAnalysis (Synaptosoft, Decatur, GA) and Clampfit 10 (Molecular Devices). The kinetics of IPSCs were obtained using Clampfit 10 (Molecular Devices). The conductance (g) underlying IPSCs was calculated from $g = IPSC_{peak}/(V_m - EGABA_A)$, where $IPSC_{peak}$ is the peak amplitude of the IPSC and V_m is the holding voltage. The equilibrium potential of $GABA_A$ current ($EGABA_A$) was estimated from the Nernst equation (Nernst 1888) and the relative permeabilities of Cl^- and HCO_3^- through $GABA_A$ receptors (Staley et al. 1995): $EGABA_A = (RT/F)*\ln[([Cl^-]_i + 0.2[HCO3^-]_i)/([Cl^-]_o + 0.2[HCO3^-]_o)]$, where R is the gas constant, T is the temperature, F is the Faraday constant, $[\ ]_i$ is the intracellular ionic concentration, and $[\ ]_o$ is the extracellular ionic concentration. Synthetic IPSPs and their patterning of potentials were analyzed using Clampfit 10 and Origin 7 (Microcal Software, Northampton, MA).

Statistics

Data are reported as means ± SD. Paired and unpaired datasets were compared using the nonparametric Wilcoxon signed-rank (WSR) and Mann-Whitney U test (MWU) tests, respectively. Data were considered significantly different if $P < 0.05$. Descriptive and comparative statistics were generated using Origin 7, Igor Pro 6 and Prism 4 (GraphPad Software, La Jolla, CA).

RESULTS

Connectivity of single GP neurons and estimation of the total number of GP-STN terminals

Serial sections of 10 GP neurons that were juxtacellularly filled in vivo with neurobiotin were first examined in the light microscope. Each neuron was labeled by a dense brown DAB or black (Ni^{2+}/DAB) reaction product (Fig. 1). As described previously, rat GABAergic GP neurons could be divided into

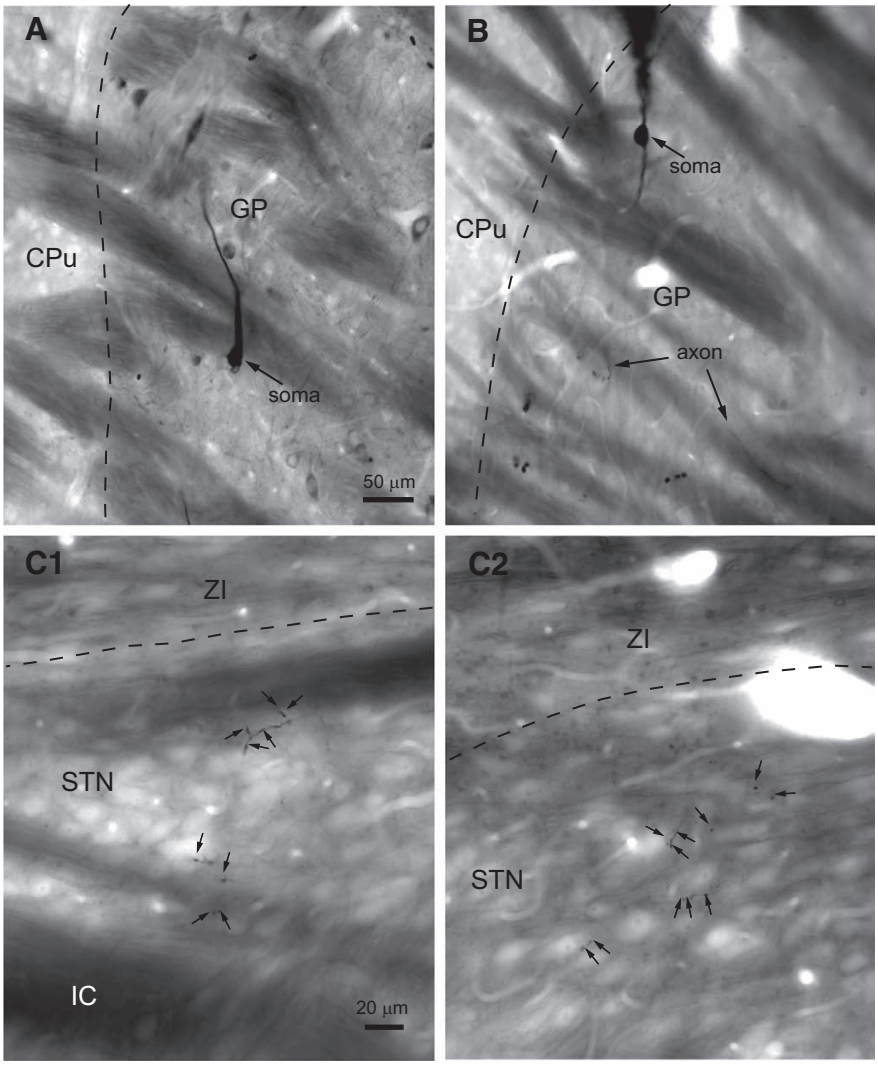

FIG. 1. Individual globus pallidus (GP neurons form sparse terminal fields in the subthalamic nucleus (STN). *A* and *B*: light micrographs of single GP neurons that were juxtacellularly labeled in vivo. In *A,* the tissue has also been immunolabeled for parvalbumin, which is expressed by a subpopulation of neurons in the GP. The juxtacellularly labeled GP neuron, which was revealed using diaminobenzidine (DAB) in the presence of Ni^{2+}, is easily distinguished from parvalbumin immunoreactive neurons, which were revealed using DAB, on the basis of labeling intensity and color (not apparent here). *C, 1* and *2*: labeled axonal boutons (small arrows) arising from a GP axon occurred in small clusters that were distributed at low density across the STN. The dashed lines mark the boundary between the striatum (CPu) and GP in *A* and *B* and the boundary between the zona incerta (ZI) and the STN in *C1* and *C2*. The internal capsule (IC) underlying the STN is visible in *C1*. Scale in *A* also applies to *B*. Scale in *C1* also applies to *C2*.

two classes on the basis of their axonal projections (Bevan et al. 1998; Kita and Kitai 1994). Each GP neuron possessed local axon collaterals and projected to the entopeduncular nucleus, STN and substantia nigra, but two of these neurons also projected to the striatum. It is likely that the GP-STN connection of each neuron was labeled in its entirety because more distal collaterals were also strongly labeled. As GP-STN axonal boutons formed synaptic contacts when examined by electron microscopy, they were assumed to be synaptic terminals. The number of GP-STN axon terminals arising from single neurons were similar in Wistar and Sprague-Dawley rats (Wistar = 246 ± 128 terminals, $n = 6$ neurons; Sprague-Dawley = 238 ± 147 terminals, $n = 4$ neurons). Thus the data were pooled, yielding a mean of 243 ± 147 (range, 46–455) terminals per GP neuron. Although the range of data was large, the distribution of data across the sample population was not significantly different from a Gaussian distribution (Shapiro-Wilk test, $P = 0.444$).

Stereological estimation of the number of rat GP neurons is 46,000 (Oorschot 1996). Although basal forebrain cholinergic neurons are also present in the GP, physiological and anatomical studies suggest that these neurons comprise ~5% of the neurons in the GP (Cooper and Stanford 2000; Gritti et al. 2006; Zaborsky et al. 1999). As the majority (~95%) of GP neurons are GABAergic neurons that project within the basal ganglia, the total number of GP-STN terminals was estimated to be 10.6 million (46,000 GP neurons × 0.95 × 243 terminals per GP-STN neuron).

Stereological estimation of the total number of GP-STN synapses

GP neurons possess axon terminals that, in some cases, appear to possess multiple sites of neurotransmitter release (synapses) (Bevan et al. 1997; Smith et al. 1990). Therefore the total number of GP-STN synapses may be greater than the total number of GP-STN terminals. To determine the total number of GP-STN synapses, the volume of the STN and the density of GP-STN synapses were estimated using the Cavalieri and dissector techniques, respectively (West 1999). Analysis of Wistar and Sprague-Dawley rats revealed that the volume of the STN in the two strains was similar (Wistar = 0.241 ± 0.032 mm^3, $n = 2$ rats, 4 hemispheres; Sprague-Dawley = 0.211 ± 0.018 mm^3, $n = 2$ rats, 4 hemispheres). The data were therefore pooled, and the volume of the STN was estimated to be 0.226 ± 0.029 mm^3.

Four blocks of STN tissue were prepared from 70-μm sections taken from the animals in which the Cavalieri technique was applied. Ultrathin sections were then taken from each block and labeled for GABA immunoreactivity using the postembedding immunogold technique. Adjacent pairs of sections were examined and photographed at a magnification of ×15,000–20,000. The dissector technique was then applied to estimate the density of GABA-immunoreactive symmetrical synapses in the STN (Fig. 2). Although the GP is the predominant source of GABAergic terminals in the STN, the mesopontine tegmentum provides a minor GABAergic input to the STN (Bevan and Bolam 1995; Bevan et al. 1995). However, these two afferents may be distinguished on the basis of morphological properties because GP-STN synapses are symmetric and those derived from the brain stem are asymmetric (Bevan and Bolam 1995; Bevan et al. 1995, 1997; Smith et al. 1990). Thus estimates of the density of symmetrical GABAergic synapses approximate the density of GP-STN synapses. Approximately 200 μm^3 of the STN was sampled in each block. The densities of GABAergic synapses in the STN of Wistar rats and Sprague-Dawley rats were similar (Wistar = 55.7 ± 22.0 million mm^{-3}, $n = 2$ blocks; Sprague-Dawley = 50.5 ± 15.2 million mm^{-3}, $n = 2$ blocks). Therefore the data were pooled and the density of GP-STN synapses was estimated to be 53.1 ± 15.7 million mm^{-3}. The total number of GP-STN synapses [calculated from the volume of the STN (0.226 ± 0.029 mm^3) multiplied by the density of GABAergic GP-STN synapses (53.1 ± 15.7 million mm^{-3})] was therefore estimated to be 12.0 million. Because the number of GP-STN synapses (12.0 million) is greater than the number of GP-STN terminals (10.6 million) these data confirm that some GP-STN terminals form more than one synapse.

Estimation of divergence and convergence in the GP-STN connection

Using the figures derived above, it is possible to calculate that an individual GP neuron forms ~275 synapses in the STN (12.0 million synapses/(46,000 × 0.95) GP neurons]. Stereological analyses have shown that the rat STN contains 13,600 neurons (Oorschot 1996). Thus if each GP synapse was formed with a different STN neuron, an individual GP neuron would contact ~275 neurons, i.e., 2.0% of all STN neurons. As the average number of GP synapses per STN neuron is 883 (12.0 million synapses/13,600 STN neurons), the maximum number of GP neurons that could provide synaptic input onto a single STN neuron is also 883, which represents 2.0% of the 43,700 GP neurons that innervate the STN. Together these figures, which represent the maximum degrees of divergence and convergence, demonstrate that an individual GP neuron innervates a small proportion of STN neurons and that an individual STN neuron receives inputs from a similarly limited fraction of GP neurons.

Spatial distribution of synaptic terminals arising from individual GP neurons

The figures estimated in the previous section define an upper limit on the degree of divergence and convergence in the GP-STN connection. However, individual GP neurons may form multiple synaptic contacts with an individual STN neuron because as stated in the preceding text, individual GP-STN terminals may form multiple contacts with the same postsynaptic neuron and multiple GP-STN terminals arising from individual GP neurons may terminate on the same postsynaptic neuron. Indeed, multiple GP-STN terminals arising from a single GP neuron often clustered around individual STN neurons (Fig. 1).

To test for clustering of GP-STN terminals, the terminal distributions arising from the 10 labeled GP neurons were compared with an equal number of terminals arranged at random within an equivalent three-dimensional space. For each GP neuron, the GP-STN terminal field possessed a greater proportion of extreme interterminal distances than the simulated random field (e.g., Figs. 3, *A* and *B*, and S1, *A* and *B*).[1] Indeed, the average distance between nearest neighboring ter-

[1] The online version of this article contains supplemental data.

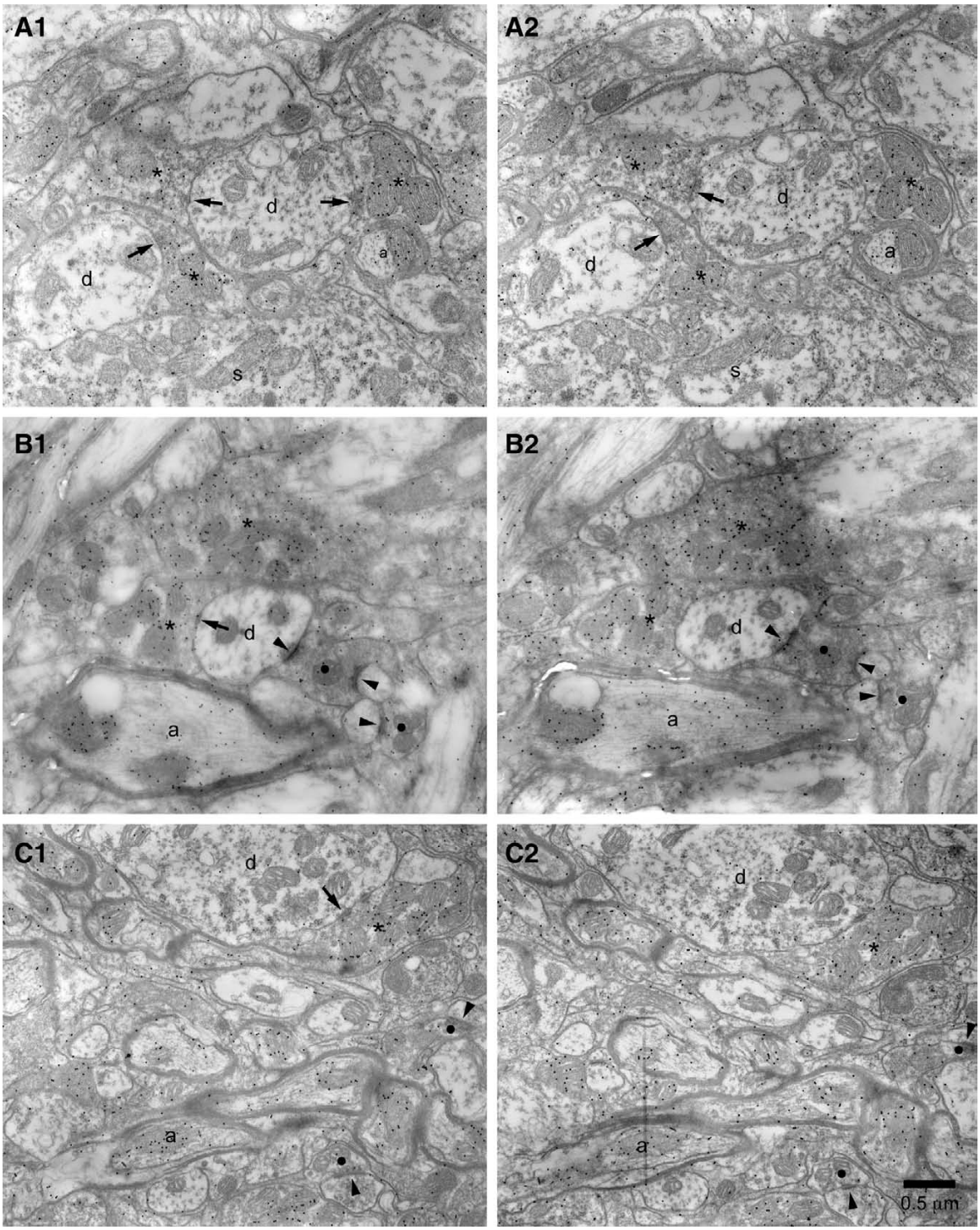

FIG. 2. Estimation of the density of GABA-immunoreactive GP-STN synapses. *A–C, 1 and 2*: examples of pairs of adjacent ultrathin sections in which GABA-immunoreactive symmetrical synaptic contacts (arrows) were "counted" using the dissector technique, i.e., they were present in the "reference" section (*A1, B1, C1*) but not in the adjacent "look-up" section (*A2*, *B2*, *C2*). Note the relatively high density of immunogold particles in terminals (*) that form symmetrical synaptic contacts compared with immunonegative structures such as terminals (●) that form asymmetric synaptic contacts (arrowhead) or the dendrites (d) or somata (s) of STN neurons. Two GABA-immunoreactive terminals formed symmetrical synapses in both sections (*A*) and were therefore not counted. Myelinated GABA-immunoreactive axons (a) are also present in some micrographs (*B* and *C*). Scale bar in *C2* applies to each panel.

minals was significantly smaller for GP-STN than simulated fields (Figs. 3*C* and S1*C*; GP-STN = 8.8 ± 3.2 μm, n = 10 fields; randomly distributed fields = 19.2 ± 2.3 μm, n = 10 simulated fields, with each simulated field representing an average of 10 "runs"; WSR test, P = 0.0019). Nearest neighbor frequency distributions for GP-STN and simulated fields (normalized to the total number of nearest neighbor distances for each field) were well fitted by log normal plots with peaks of 3.5 and 14.8 μm, respectively (Fig. 3*C*; for GP-STN fields, χ^2 = 3.63, df = 27, P = 0.99; for simulated fields, χ^2 = 20.13,

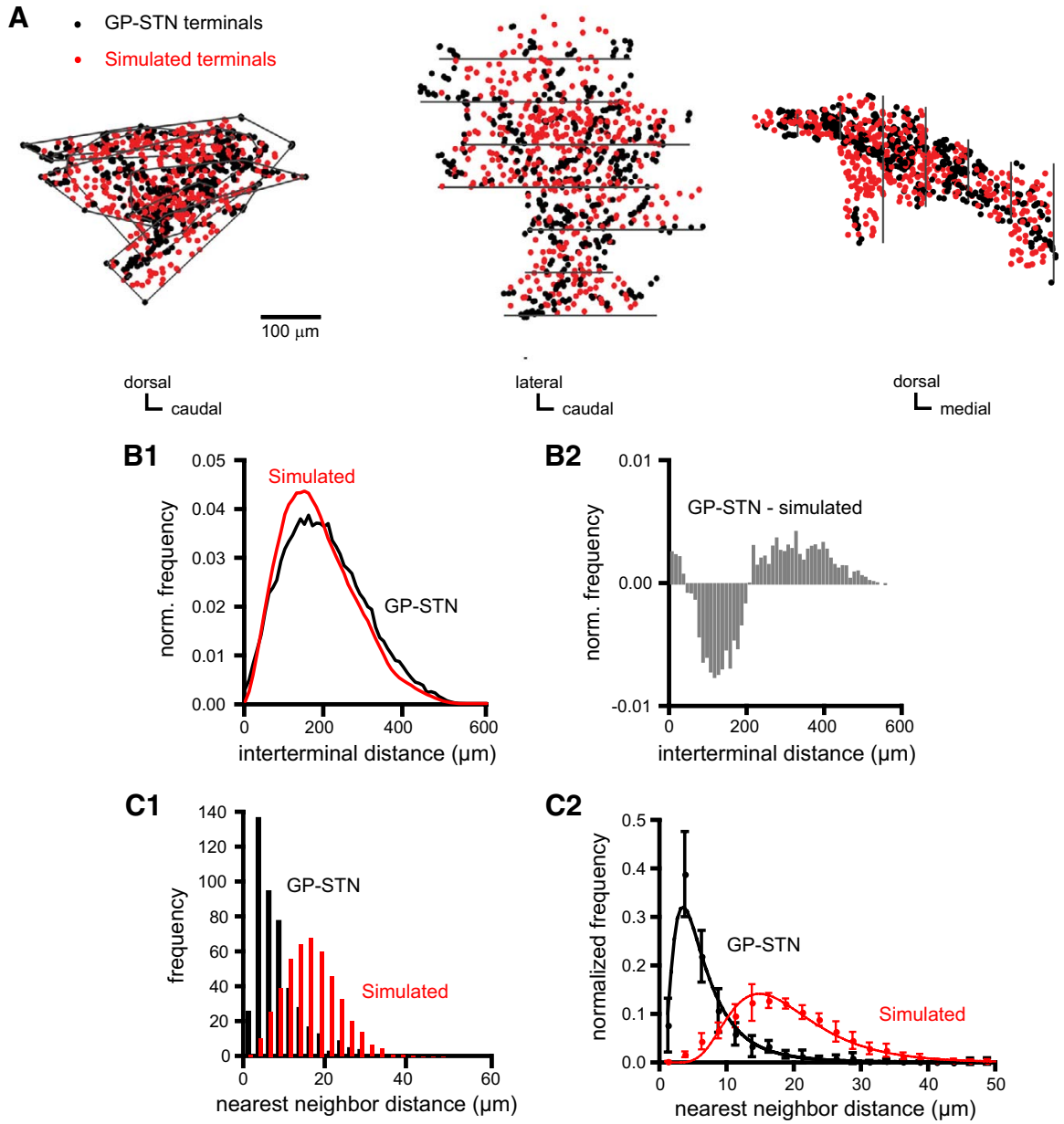

FIG. 3. Three-dimensional distribution of GP-STN terminals. *A*: sagittal, horizontal and coronal projections (*left, middle,* and *right,* respectively) of a GP-STN terminal field that arose from a single labeled GP neuron. Each black dot represents 1 of 455 labeled GP-STN terminals. Red dots represent an equivalent number of terminals that have been arranged at random (simulated) within the volume occupied by the GP-STN terminal field, the boundaries of which are indicated (for each tissue section) by gray lines. *B1*: comparison of frequency histograms of all interterminal distances for GP-STN (black) and simulated (red) terminal fields indicates that the GP-STN field possessed a greater proportion of interterminal distances at the extremes of the distribution. *B2*: subtraction of the simulated field from the GP-STN field confirmed this trend. *C1*: the distance between nearest neighboring terminals was smaller for the GP-STN terminal field (black) than the simulated field (red). *C2*: population data from 10 labeled GP neurons confirms that the distance between nearest neighboring terminals was smaller for GP-STN than simulated terminal fields. GP-STN and simulated fields were well fit by a log normal distribution with peaks at 3.5 and 14.8 μm, respectively.

df = 36, $P = 0.98$). Thus GP-STN terminals are arranged in a spatially heterogeneous, clustered pattern.

Correlated light and electron microscopic analyses were then utilized to test the hypothesis that terminal clusters represented multiple synaptic contacts between individual GP axons and single STN neurons. Two regions of the STN derived from two animals were examined (Figs. 4 and S2). In the first tissue block (derived from a Sprague-Dawley rat), 11 boutons were examined by correlated light and electron microscopy (Fig. 4). Each bouton identified at the light microscopic level corresponded to a synaptic terminal. Six terminals established symmetrical synaptic contacts with the soma and proximal dendrite of a single STN neuron. The other terminals established contacts with dendrites that may have arisen from the same or different STN neurons. Three of these other terminals established synaptic contacts with a single dendrite. Another terminal and a nonvaricose section of axon established synaptic contacts with another dendrite, and a further dendrite received synaptic input from a single labeled terminal. Although previous reports have suggested that individual GP terminals possess multiple active zones (Bevan et al. 1997; Smith et al. 1990) it was not possible to conclusively distinguish between

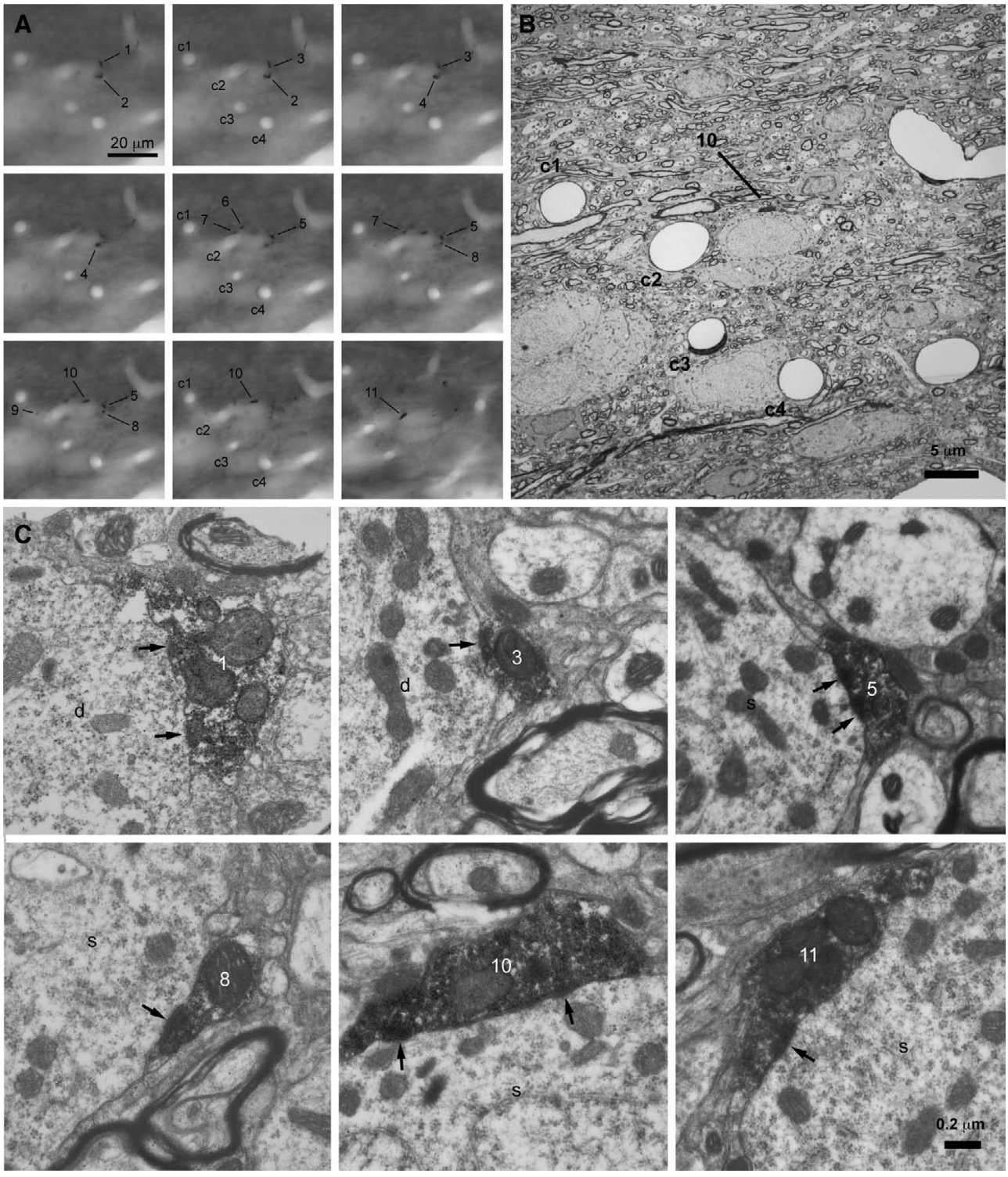

FIG. 4. Individual GP axons often form multiple synaptic contacts with individual STN neurons. *A–C*: correlated light (*A*) and electron microscopic (*B* and *C*) analyses of a cluster of GP-STN terminals that arose from an individual GP neuron. *A*: from left to right, through-focus light micrographs of a cluster of labeled GP-STN terminals (1–11). Capillaries (c1–c4) act as points of registration between the light and electron micrographic images. *B*: a low-magnification electron micrograph of the region in *A*. *C*: high-magnification electron micrographs of 6 terminals (1, 3, 5, 8, 10, 11) that formed symmetrical synaptic contacts (arrows) with a proximal dendrite (d) and soma (s) of a single STN neuron. The other terminals formed synaptic contacts with other STN dendrites (not illustrated). The scales in *A* and *C* apply to all panels in *A* and *C*, respectively.

irregularly shaped contiguous synapses and separate synapses due to the dense terminal labeling. In a second tissue block (derived from a Wistar rat), 11 boutons were examined (Fig. S2). Each bouton identified at the light microscopic level corresponded to a synaptic terminal. Five terminals established symmetrical synaptic contacts with the soma of a single STN neuron. The other terminals established contacts with dendrites that may have arisen from the same or different STN neurons.

Three terminals synapsed with a single dendrite and 3 terminals synapsed individually with different dendrites. Thus of the 23 synaptic connections that arose from 22 terminals and 1 nonvaricose section of axon, ≥19 (82.6%) formed one of several contacts with an individual postsynaptic element. Together, these data demonstrate that individual GP neurons commonly form multiple synaptic contacts with both the somatic and dendritic compartments of individual STN neurons.

Another remarkable feature of the GP-STN connection is the spatially distributed nature of the clusters of GP-STN terminals that arise from individual GP neurons. This can be appreciated qualitatively from Fig. S3 in which the large expanse of the terminal fields arising from the two GP neurons considered in the preceding text have been mapped relative to the nuclear boundaries of the STN. Thus the average maximal extent of the GP-STN terminal fields arising from single neurons was 679.9 ± 250.3 μm (range, 224.8–1,068.5 μm, $n = 10$). The average maximal extents of the terminal field in the rostral-caudal, medial-lateral and dorsal-ventral axes were 657.0 ± 203.3 μm (range, 391.3–936.5 μm), 365.3 ± 156.6 μm (range, 173.1–742.7 μm), and 286.2 ± 63.1 μm (range, 192.5–351.4 μm), respectively. As the rat STN possesses rostral-caudal and medial-lateral axes up to ~1,000 μm in length and a dorsal-ventral axis up to ~400 μm in length, GP-STN connections arising from single GP neurons span a large extent of the STN.

The spatially distributed nature of GP-STN terminal fields was confirmed by calculating the proportion of the STN that each field occupied using the Cavalieri technique to estimate the volume of the terminal field at its maximal extents and the volume of the STN in each animal. Here again, data from Wistar and Sprague-Dawley rats were pooled because the field volumes (expressed as percentages of STN volume) were similar (Wistar = 4.1 + 2.8%, $n = 6$; Sprague-Dawley = 3.3 + 2.6%, $n = 4$). Although an individual GP neuron represents only 0.0023% of GP neurons, the average volume of the STN occupied by each terminal field was 3.8 ± 2.6% (range, 0.95–8.49%). Taken together, the data demonstrate that the axon terminals of individual GP neurons are arranged in small clusters that are sparsely distributed across a large extent of the STN. Furthermore, because single GP axons often form multiple synaptic contacts with single STN neurons, the degree of divergence and convergence in the GP-STN connection is likely to be considerably more restricted than the 2% connectivity estimated in the previous section.

Physiological properties of the GP-STN connection

To investigate the physiological properties of the GP-STN connection, $GABA_A$ receptor-mediated GP-STN transmission was studied using patch-clamp recording of STN neurons in brain slices. Given that the GP represents by far the major source of GABAergic inputs to STN neurons (Bevan et al. 1995; Shink et al. 1996; Smith et al. 1990, 1998), it was assumed that the majority of evoked IPSCs and mIPSCs arose from GP-STN axons.

SINGLE GP-STN AXONS COMMUNICATE WITH SINGLE STN NEURONS VIA MULTIPLE SYNAPSES. The structural organization of the GP-STN connection elucidated above suggests that single GP-STN axons often communicate with single STN neurons through multiple sites of transmitter release. To determine whether GP-STN axons exhibit corresponding physiological properties, the minimal stimulation technique was employed to evoke transmission from single GP-STN axons (Fig. 5). Gradually increasing the amplitude of stimulation in 0.5- to 10-μA steps led to the generation IPSCs with a distinct threshold. At stimulation threshold, large IPSCs of variable amplitudes were interspersed with complete failures in transmission (Fig. 5, *A* and *B*). In some cases, it was possible to further increase the amplitude of stimulation beyond threshold so that the number of transmission failures declined but the mean amplitude of minimally evoked IPSCs remained constant. The peak conductances underlying the mean and maximal responses evoked by

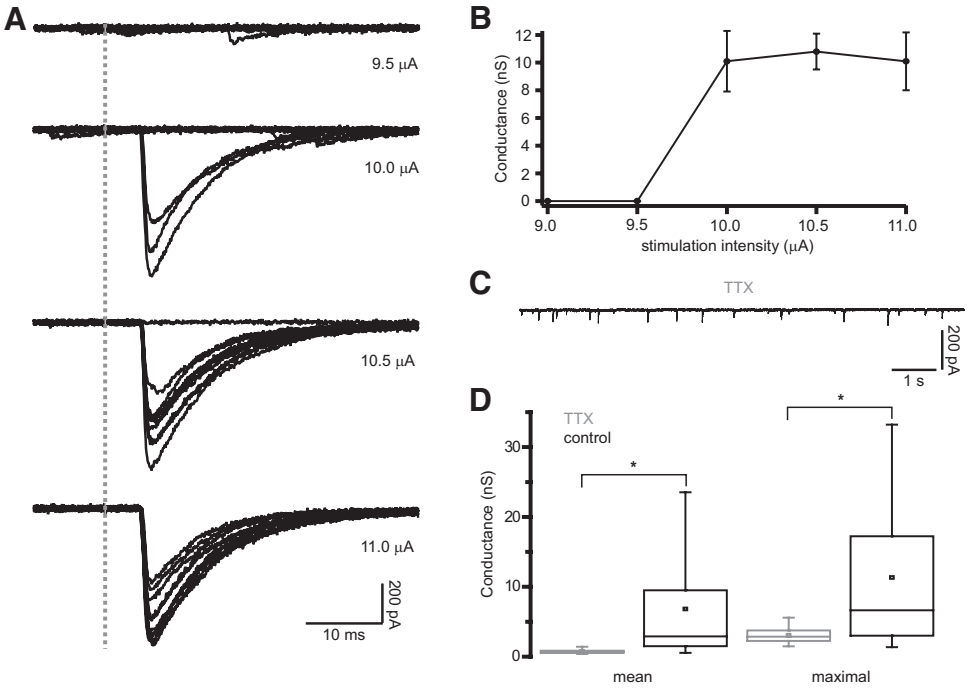

FIG. 5. Minimally evoked inhibitory postsynaptic currents (IPSCs) are significantly larger than miniature IPSCs (mIPSCs) in STN neurons. *A*: responses evoked in a single STN neuron to electrical stimulation of the internal capsule with gradually increasing intensity (10 superimposed trials in each panel; onset of stimulation denoted by the gray dashed line). *A* and *B*: at 10 μA a large IPSC was evoked in 3 of 10 trials. As the stimulation intensity was increased the number of transmission failures decreased but the mean amplitude of minimally evoked IPSCs remained constant. The sharp threshold and consistent latencies, mean amplitudes and kinetics of the evoked IPSCs suggest that they result from minimal stimulation, that is, stimulation of a single GP-STN axon. The large and variable amplitude of minimally evoked IPSCs compared with those observed in the presence of TTX (*C* and *D*) suggest that single GP-STN axons transmit via several synapses. *C*: representative recording of mIPSCs in the presence of 1 μM TTX. The current scales in *A* and *C* are identical for comparison. *D*: the mean and maximal amplitudes of minimally evoked IPSCs ($n = 24$ neurons) were significantly greater than mIPSCs recorded in the presence of TTX ($n = 17$ neurons). Asterisk, $P < 0.05$.

minimal stimulation were calculated to be, respectively, 6.82 ± 7.19 nS (range = 0.51–25.33 nS, $n = 24$) and 11.32 ± 10.61 nS (range = 1.08–41.9 nS, $n = 24$). To compare the conductances underlying putative single axon responses and transmission at single GP-STN synapses, $GABA_A$ receptor-mediated mIPSCs were recorded in the presence of the selective Na_v channel blocker tetrodotoxin, TTX (Fig. 5, *C* and *D*). mIPSCs occurred at a frequency of 3.1 ± 1.7 Hz ($n = 17$ neurons) and were associated with significantly smaller mean and maximal conductances (mean conductance = 0.73 ± 0.26 nS, range = 0.38–1.42 nS, $P < 0.001$, MWU test; maximal conductance = 3.06 ± 1.10 nS, range = 1.48–5.59 nS, $P < 0.009$, MWU test). Because the conductances associated with miniature transmission were significantly smaller than the conductances generated by minimal stimulation, the physiological data support the view that individual GP-STN axons communicate with individual postsynaptic STN neurons through the release of GABA at multiple synaptic connections.

NEIGHBORING STN NEURONS RARELY RECEIVE COMMON GP-STN INPUTS. The structural organization of the GP-STN connection elucidated in the preceding text suggests that STN neurons rarely share inputs from the same GP-STN axon. To determine whether GP-STN axons possess corresponding physiological properties, neighboring STN neurons (within 25 μm of each other) were recorded simultaneously in the whole cell voltage-clamp configuration during the minimal stimulation of a putative, single GP-STN axon (Fig. 6, *A–C*). Given their close proximity, neighboring neurons were likely to reside in a homologous functional territory and to have received a similar degree of deafferentation during slice preparation. Gradually increasing the intensity of electrical stimulation in 2–10 μA steps led in each case to the sudden appearance of an evoked IPSC in only one neuron of each neuron pair tested (7 pairs). The magnitude of the evoked IPSC varied considerably in amplitude from trial to trial. Thus large, intermediate-sized IPSCs and apparent failures of transmission were observed. In five pairs of neurons, the poles of electrical stimulation were then altered and the intensity of stimulation was again gradually increased until responses were first detected. For some combinations of electrodes, minimal stimulation evoked IPSCs in the previously unresponsive neuron but not in the previously responsive neuron (3 pairs). Taken together, these data suggest that neighboring STN neurons rarely receive common $GABA_A$ receptor-mediated inputs from the same GP-STN axons.

IMPACT OF THE GP-STN CONNECTION ON AUTONOMOUS STN ACTIVITY. GABAergic inputs from the GP have previously been shown to reset the autonomous firing of postsynaptic STN neurons through membrane hyperpolarization and the subsequent deactivation of postsynaptic Na_v channels and thus have the potential to powerfully synchronize STN activity (Baufreton et al. 2005; Bevan et al. 2002). To estimate the number of synaptic inputs that are required for resetting and synchronization, the dynamic-clamp technique (Robinson and Kawai 1993; Sharp et al. 1993) was utilized to synthesize a range of $GABA_A$ receptor-mediated inputs from the GP. The magnitude and kinetics of the underlying synaptic conductance waveforms were guided by our anatomical data and measurements of minimally evoked and miniature GP-STN transmission, described in the preceding text. Peak conductances ranged from 1 to 25 nS and thus represented activity at ~1–34

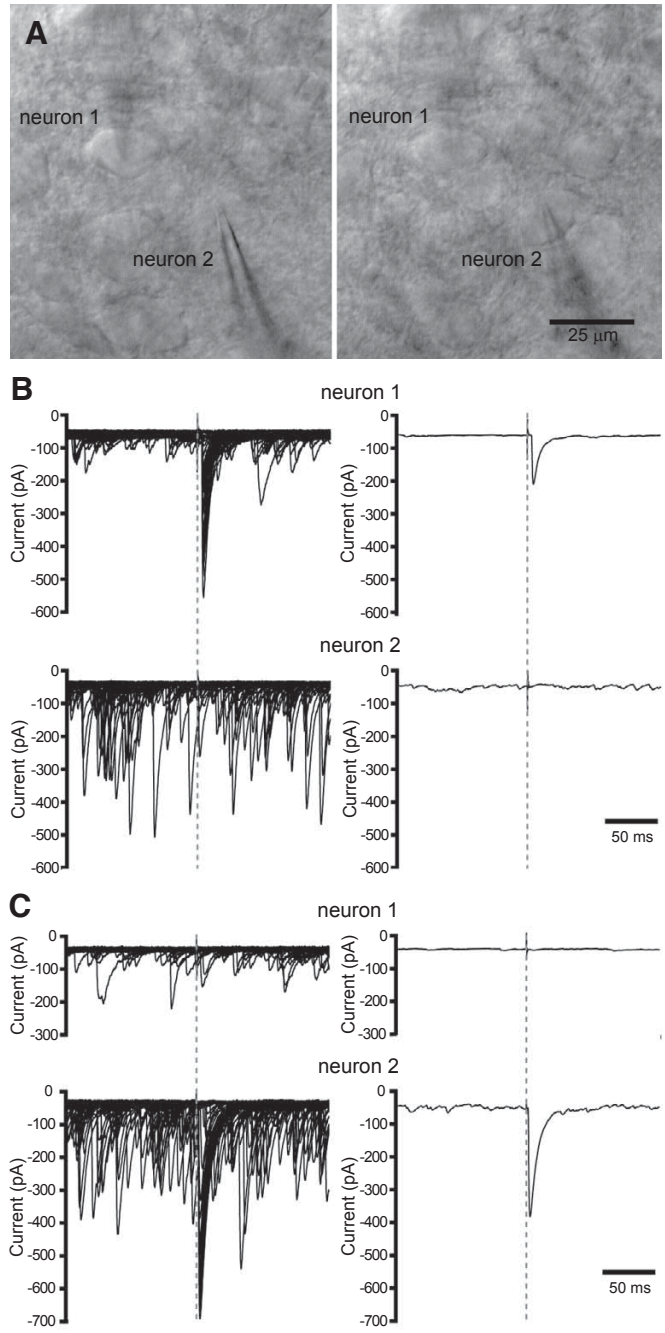

FIG. 6. Neighboring STN neurons receive inputs from different GP-STN axons. *A*: through-focus micrographs of 2 neighboring STN neurons (1 and 2) that were recorded simultaneously in the whole cell configuration. *B*: superimposed (*left*; 50 trials) and mean (*right*) responses of neurons 1 and 2 to minimal stimulation of the internal capsule. The gray dashed lines indicate the onset of electrical stimulation. Numerous spontaneous IPSCs were also detected. *C*: as for *B* except that a different combination of electrodes were chosen for minimal stimulation. Note that different neurons respond to each stimulus and that minimally evoked IPSCs varied greatly in amplitude in both neurons.

synapses. The kinetics of evoked $GABA_A$ receptor-mediated IPSCs were derived from measurements in eight STN neurons (10–90% rise time: mean = 1.1 ± 0.4 ms, range = 0.8–1.6 ms; monoexponential t_{decay}: mean = 7.8 ± 4.4 ms, range = 4.6–18.4 ms, $R = 0.94 \pm 0.02$, R range = 0.92–0.97; biexponential t_{decay}: $\mathbf{A}_1 = 87.5 \pm 5.0\%$, A_1 range = 82.5–97.0%;

t_{decay1} = 7.0 ± 3.0 ms, t_{decay1}range = 3.9–11.6 ms; A_2 = 12.5 ± 5.0%, A_2 range = 3.0–17.5%; t_{decay2} = 33.9 ± 19.7 ms, t_{decay2} range = 11.9–64.0 ms, R = 0.97 ± 0.01, R range = 0.96–0.98). On the basis of these values, two conductance waveforms were generated, each possessed a 10–90% rise time of 0.8 ms but differed slightly in their decay kinetics. One waveform decayed with monoexponential kinetics (t_{decay} = 10 ms), whereas the other waveform decayed with biexponential kinetics (the relative amplitude and time constants of decay were A_1 = 89.7%, t_{decay1} = 7 ms, A_2 = 10.3%, t_{decay2} = 35 ms). The equilibrium potential of the $GABA_A$ receptor conductance was set to −84 mV, as determined by earlier studies employing gramicidin-based perforated patch recording (Bevan et al. 2000, 2002). The impact of synthetic $GABA_A$ receptor-mediated IPSPs on the autonomous activity of 7 STN neurons was studied. Five were recorded using the gramicidin-based perforated-patch configuration and two were recorded using the whole cell configuration. The data derived from conductance waveforms with different decay kinetics or different recording modes were similar and were therefore pooled.

In the presence of AMPA-kainate, NMDA, $GABA_A$, and $GABA_B$ receptor antagonists, STN neurons fired autonomously at 7.8 ± 2.6 Hz (range = 5.5–13.3 Hz). Autonomous firing was highly regular as evidenced by the low coefficient of variation (CV) of interspike intervals (CV = 0.12 ± 0.05, range = 0.06–0.20). The responses of each neuron to synthetic IPSPs were then recorded for ≥20 trials per conductance level (Fig. 7). As the conductance underlying synthetic IPSPs increased, several effects were observed: progressively longer pauses in activity both within neurons and across the sample population were generated; IPSPs more effectively reset the oscillatory cycle underlying autonomously generated action potentials, as evidenced by a progressive reduction in the

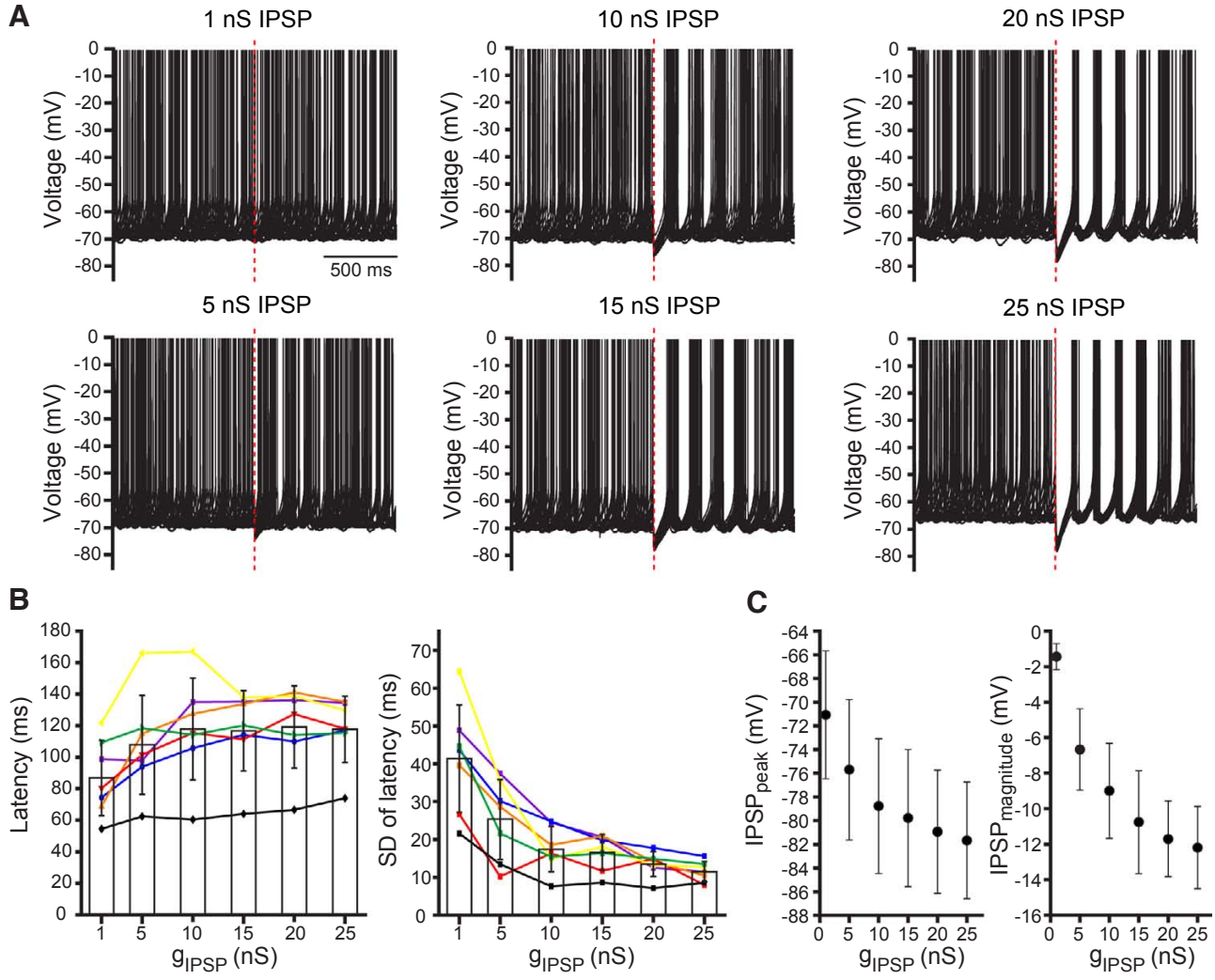

FIG. 7. Resetting of autonomous activity by synthetic GP-STN inhibition. *A*: impact of synthetic $GABA_A$ receptor-mediated IPSPs with underlying conductances of 1–25 nS on the autonomous activity of a STN neuron. Twenty superimposed trials are illustrated for each conductance. The time of onset of each IPSP is denoted by a dashed red line. A pause in activity and resetting of action potential generation is discernable for 5- to 25-nS IPSPs. The variability in the timing of action potentials generated after each IPSP decreased as the conductance increased over the 5–25 nS range. *B*: population data for the latency (*left*) and SD (*right*) of the 1st action potential generated after each IPSP plotted against the underlying conductance (g_{IPSP}). Data from each neuron tested (n = 7) are represented by a distinct color and symbol (neuron in *A* is denoted by purple lines and symbols). The color code is consistent with Fig. 8. *C*: population data for the peak hyperpolarization generated by each IPSP ($IPSP_{peak}$, *left*) and the magnitude of each IPSP ($IPSP_{magnitude}$ = membrane potential at which IPSP was evoked − $IPSP_{peak}$, *right*) plotted against the conductance underlying each IPSP. The peak of the IPSP progressively approached the equilibrium potential of the synaptic input and increased in magnitude as the conductance increased.

variability or "jitter" (SD of latency) of action potentials following each IPSP; and the magnitude and peak hyperpolarization of IPSPs increased such that at 25 nS (equivalent to ~34 synaptic inputs) the membrane potential was consistently driven within a few mV of the equilibrium potential of the $GABA_A$ receptor conductance. Given that each STN neuron receives input from ~883 GP-STN synapses, these data suggest that synchronous transmission at only a small fraction of GP-STN synapses is sufficiently powerful to reset the oscillatory cycle underlying the autonomous activity of STN neurons in vitro.

To determine the magnitude of conductances that are necessary to produce correlated/synchronized activity in STN neurons (the autonomous activity of which varies independently in frequency and rhythmicity) trials from each of the seven neurons tested above were aligned to the onset of conductance injection and population peristimulus time histograms were generated (Fig. 8). Significant correlations in activity were deemed as counts with less than or greater than the mean count $\pm 3 \times$ SD before conductance injection. Significantly correlated activity was observed for conductances of 5–25 nS (equivalent to ~7–34 synaptic inputs). Both the pauses in activity produced by each IPSP and the action potential(s) following each synthetic IPSP were significantly correlated and the degree of correlated activity progressively increased as the conductance increased from 5 to 25 nS. Together these data suggest that the autonomous activities of STN neurons can be synchronized by synchronous transmission at a small fraction of their inputs from the GP in vitro.

DISCUSSION

The findings of the present study suggest that the paucity of temporally correlated activity between the GP and STN is due to the sparsity and selectivity, rather than the potency, of GP-STN synaptic connections.

Pattern of connectivity of GP-STN axons

Because of the limitations of tract-tracing methods for the precise quantification of connectivity between regions of the brain, we employed single-neuron labeling and stereological sampling to estimate the maximal divergence and convergence in the GP-STN connection. We demonstrated that individual GP neurons maximally contact only a small proportion (2%) of STN neurons and individual STN neurons maximally receive input from a similarly small proportion (2%) of GP neurons. Comparison of GP-STN terminal fields with simulated fields confirmed that GP-STN terminals arising from individual GP neurons are arranged in clusters that are sparsely distributed

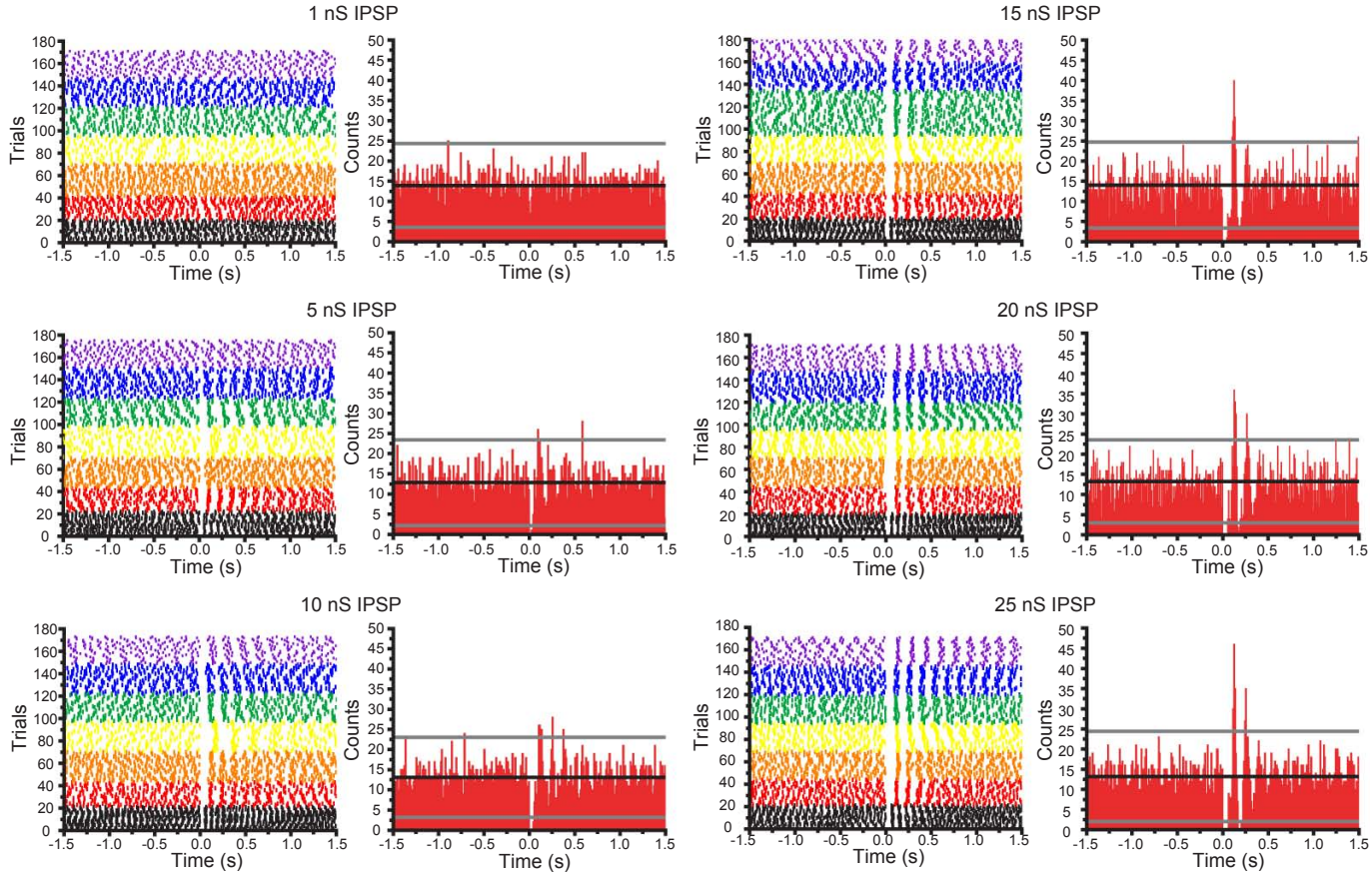

FIG. 8. Synchronization of autonomous STN activity by synthetic GP-STN inhibition. Color-coded raster plots for 7 STN neurons (color code as for Fig. 7) illustrating the action of synthetic $GABA_A$ receptor-mediated IPSPs (that were generated at 0 s with underlying conductances of 1–25 nS) on autonomous firing. A peristimulus time histogram (PSTH) is to the right of its respective raster plot. The black line on each PSTH represents the mean number of action potentials per time bin of 10 ms in the period (−1.5 to 0 s) before synthetic inhibition. The gray lines represent the mean ±3 SD of action potentials per time bin before inhibition. Correlated activity, as shown by significant peaks and troughs in the PSTHs, was observed for synthetic IPSPs with underlying peak conductances of 5–25 nS. The degree of correlation increased progressively as the conductance underlying the synthetic IPSP increased.

across large expanses of the STN. Thus most closely neighboring STN neurons are not innervated by the same GP neurons. The wide distribution and low density of innervation is similar to other axonal projections in the basal ganglia and may reflect a common design principle that minimizes correlated activity, and thus redundancy, in the firing patterns of neighboring postsynaptic neurons within homologous functional domains (Kincaid et al. 1998).

In common with other target structures of GP neurons (Bevan et al. 1997, 1998; Sadek et al. 2007; Smith and Bolam 1990), correlated light and electron microscopic analyses confirmed that clusters of GP-STN terminals arising from single GP axons often formed multiple synaptic contacts with somatic and/or dendritic domains of individual postsynaptic neurons. At least six terminals were observed in synaptic contact with an individual postsynaptic element, although this number is unlikely to represent the maximal limit of innervation. It is, however, unlikely that individual GP neurons innervate only a single STN neuron because terminals arising from single GP neurons formed clusters around the somata of multiple, widely distributed STN neurons. Furthermore, axosomatic synapses and synapses with distal dendrites were observed in close proximity and are thus unlikely to represent inputs to the same neuron. Individual GP-STN terminals may also form multiple synaptic contacts with individual STN neurons, as suggested previously (Bevan et al. 1997; Smith et al. 1990). Indeed in support of this mode of transmission, our estimate of GP-STN synaptic connections exceeded our estimate of GP-STN synaptic terminals. Unfortunately, heavy presynaptic labeling with DAB reaction product precluded a more definitive determination of the number of synaptic connections of individual GP-STN terminals.

Each identified GP neuron contacted the somata, proximal, and distal dendrites of STN neurons and therefore unlike cortical or striatal GABAergic interneurons (Klausberger and Somogyi 2008; Tepper et al. 2008), cannot be subdivided with respect to their selective innervation of postsynaptic domains. In general, axosomatic GABAergic inputs play a role in the timing of action potentials, whereas axodendritic inputs are important for locally regulating the integration of excitatory glutamatergic inputs, which are often directed to dendrites and dendritic spines (Cobb et al. 1995; Miles et al. 1996; Person and Perkel 2005). Individual GP neurons could therefore simultaneously influence multiple compartments of individual postsynaptic STN neurons and/or subserve different roles in targeted neurons by innervating distinct domains.

Physiological properties of GP-STN connections are concordant with their pattern of connectivity

Comparison of the conductances underlying minimal stimulation-evoked IPSCs and mIPSCs confirmed that minimal stimulation generated mean and maximal synaptic conductances that greatly exceeded those underlying miniature synaptic transmission. These data therefore suggest that single GP-STN axons typically communicate with individual STN neurons through transmission at multiple rather than single synapses and thus provide functional evidence in support of the anatomical data. Minimal electrical stimulation of single GP-STN axons also revealed that neighboring STN neurons largely receive inputs from different GP neurons. This observation supports the anatomical data, which demonstrated that individual GP neurons maximally make connections with only 2% of STN neurons and GP-STN terminals are sparsely distributed across the STN and thus form connections with similarly distributed postsynaptic neurons.

The dynamic-clamp data suggests that GP-STN inputs have the capability to potently reset and thus synchronize autonomous STN activity. Synthetic inhibition arising from only seven synapses (5 nS) interrupted STN activity and partially reset its phase. Over the 7–34 synapse range (5–25 nS), inhibition was progressively more effective—the peak of the synthetic IPSP was driven closer and more consistently to the equilibrium potential of $GABA_A$ receptor current, which presumably led to more consistent deactivation of Na_v channels that underlie autonomous firing (Baufreton et al. 2005; Beurrier et al. 2000; Bevan and Wilson 1999; Do and Bean 2003). Inhibition representative of transmission at only 14–21 GP-STN synapses had a near maximal impact on resetting and synchronization. Given that each STN neuron receives almost 900 GP-STN inputs, the data suggest that the GP-STN connection is potent and that there is a massive reserve of GABAergic inhibition in the STN. Because the conductances underlying miniature GABAergic transmission in the STN are similar to those seen in other brain regions (Kraushaar and Jonas 2000; Pedroarena and Schwarz 2003), the potency of GP-STN inhibition is likely to be a reflection of the high-input resistance of STN neurons (Carter and Regehr 2002) and the hyperpolarized equilibrium potential of $GABA_A$ receptor-mediated current (Bevan et al. 2002). The apparent potency of GP-STN inhibition, as suggested by our rudimentary dynamic-clamp studies, should, however, be further qualified. GP-STN synaptic transmission is subject to activity-dependent depression. At 10- and 50-Hz transmission, the amplitude of the steady-state IPSC depresses to ~61 and 44%, respectively, of its initial level (Baufreton and Bevan 2008). Given that rodent GP neurons discharge in this frequency range in vivo (Magill et al. 2000; Urbain et al. 2000), both the potency of unitary synaptic connections and the maximal level of inhibition may be reduced considerably. Presynaptic dopaminergic neuromodulation, which reduces the probability of transmitter release, may similarly moderate the potency of GP-STN transmission in vivo (Abbott and Regehr 2004; Baufreton and Bevan 2008; Shen and Johnson 2000). Ongoing inhibitory and excitatory synaptic activity in vivo could also limit or modify the effectiveness of GP-STN synaptic inputs (Destexhe et al. 2003), although other studies suggest that the level and impact of synaptic activity in vivo may be less substantial (Margrie et al. 2002; Waters and Helmchen 2006). Finally, application of the dynamic clamp technique to the soma more closely mimics somatic and proximal rather than distal dendritic GP-STN synaptic inputs. Given the proximity of somatic and proximal dendritic GP-STN inputs to axonal Na_v channels that underlie autonomous activity (Atherton et al. 2008), the dynamic clamp technique, as applied here, may therefore have simulated the most effective inhibitory inputs.

Implications for GP-STN activity

The sparse but selective and potent innervation by single GP neurons of a small fraction of STN neurons that are widely

distributed across the nucleus is likely to be of fundamental significance for the level of correlated firing in GP and STN neurons in vivo (Terman et al. 2002). The data suggest that the GP-STN connection is sufficiently potent to produce correlated STN activity but is so sparse and selective that technologies that sample neuronal activity at low density (Buzsaki 2004) have a low probability of recording connected GP and STN neurons (Magill et al. 2000; Mallet et al. 2008a; Raz et al. 2000; Urbain et al. 2000; Wichmann et al. 1994). In contrast, the relatively promiscuous connectivity of cultured networks may have facilitated the detection of correlated activity in organotypic co-cultures (Plenz and Kital 1999) but not ex vivo preparations of the GP and STN (Loucif et al. 2005).

In PD widespread correlated activity emerges in GP and STN neurons. The most common form is synchronization of STN neurons in the 13–30 Hz (β) band (Brown et al. 2001; Levy et al. 2000, 2001; Mallet et al. 2008b). The highly selective, restricted connectivity of the GP-STN connection implies that GP neurons must themselves be broadly synchronized if they are to participate in the pathological synchronization of STN neurons. A candidate mechanism is cortical β band activity that induces widespread but weak synchronization of STN neurons, which, in turn, excite and synchronize GP neurons, which, through feedback inhibition, further synchronize STN neurons and enhance their excitation by the cortex (Baufreton et al. 2005). Recent recordings from the parkinsonian GP-STN network in vivo support this mechanism (Mallet et al. 2008a). The loss of presynaptic dopaminergic neuromodulation of GP-STN connections in PD may additionally enhance correlated activity (and the probability of its detection) by increasing the initial probability of transmitter release from GP-STN terminals and thus maximizing (at least phasically) the strength of GP-STN transmission (Baufreton and Bevan 2008; Shen and Johnson 2000).

In conclusion, the sparse and selective connectivity we define here is likely to be a major determinant of the decorrelated activity pattern of the GP-STN network during normal rest. Additionally, we show that GP-STN transmission could theoretically exert a potent but discrete synchronizing influence, which appropriately constrained, could be important for more dynamic behavior. The nature of the connection also suggests that excessively synchronized GP output, as arises in PD, may be a key factor in the pathological hyper-synchronization of the STN.

GRANTS

This study was supported by National Institute of Neurological Disorders and Stroke Grants NS-041280 and NS-040705, the Wellcome Trust and the National Parkinson Foundation to M. D. Bevan, the MRC UK to P. J. Magill/J. P. Bolam, Parkinson's Disease Society UK Grant G-0806 to P. J. Magill and L'Association France Parkinson to J. Baufreton.

REFERENCES

Abbott LF, Regehr WG. Synaptic computation. *Nature* 431: 796–803, 2004.

Albin RL, Young AB, Penney JB. The functional anatomy of basal ganglia disorders. *Trends Neurosci* 12: 366–375, 1989.

Atherton JF, Wokosin DL, Ramanathan S, Bevan MD. Autonomous initiation and propagation of action potentials in neurons of the subthalamic nucleus. *J Physiol* 586: 5679–5700, 2008.

Baufreton J, Atherton JF, Surmeier DJ, Bevan MD. Enhancement of excitatory synaptic integration by GABAergic inhibition in the subthalamic nucleus. *J Neurosci* 25: 8505–8517, 2005.

Baufreton J, Bevan MD. D2-like dopamine receptor-mediated modulation of activity-dependent plasticity at GABAergic synapses in the subthalamic nucleus. *J Physiol* 586: 2121–2142, 2008.

Benabid AL. Deep brain stimulation for Parkinson's disease. *Curr Opin Neurobiol* 13: 696–706, 2003.

Bergman H, Wichmann T, Karmon B, DeLong MR. The primate subthalamic nucleus. II. Neuronal activity in the MPTP model of parkinsonism. *J Neurophysiol* 72: 507–520, 1994.

Beurrier C, Bioulac B, Hammond C. Slowly inactivating sodium current (I(NaP)) underlies single-spike activity in rat subthalamic neurons. *J Neurophysiol* 83: 1951–1957, 2000.

Bevan MD, Bolam JP. Cholinergic, GABAergic, and glutamate-enriched inputs from the mesopontine tegmentum to the subthalamic nucleus in the rat. *J Neurosci* 15: 7105–7120, 1995.

Bevan MD, Booth PA, Eaton SA, Bolam JP. Selective innervation of neostriatal interneurons by a subclass of neuron in the globus pallidus of the rat. *J Neurosci* 18: 9438–9452, 1998.

Bevan MD, Clarke NP, Bolam JP. Synaptic integration of functionally diverse pallidal information in the entopeduncular nucleus and subthalamic nucleus in the rat. *J Neurosci* 17: 308–324, 1997.

Bevan MD, Francis CM, Bolam JP. The glutamate-enriched cortical and thalamic input to neurons in the subthalamic nucleus of the rat: convergence with GABA-positive terminals. *J Comp Neurol* 361: 491–511, 1995.

Bevan MD, Magill PJ, Hallworth NE, Bolam JP, Wilson CJ. Regulation of the timing and pattern of action potential generation in rat subthalamic neurons in vitro by $GABA_A$ IPSPs. *J Neurophysiol* 87: 1348–1362, 2002.

Bevan MD, Wilson CJ. Mechanisms underlying spontaneous oscillation and rhythmic firing in rat subthalamic neurons. *J Neurosci* 19: 7617–7628, 1999.

Bevan MD, Wilson CJ, Bolam JP, Magill PJ. Equilibrium potential of GABA(A) current and implications for rebound burst firing in rat subthalamic neurons in vitro. *J Neurophysiol* 83: 3169–3172, 2000.

Brown P, Oliviero A, Mazzone P, Insola A, Tonali P, Di Lazzaro V. Dopamine dependency of oscillations between subthalamic nucleus and pallidum in Parkinson's disease. *J Neurosci* 21: 1033–1038, 2001.

Buzsaki G. Large-scale recording of neuronal ensembles. *Nat Neurosci* 7: 446–451, 2004.

Carter AG, Regehr WG. Quantal events shape cerebellar interneuron firing. *Nat Neurosci* 5: 1309–1318, 2002.

Cobb SR, Buhl EH, Halasy K, Paulsen O, Somogyi P. Synchronization of neuronal activity in hippocampus by individual GABAergic interneurons. *Nature* 378: 75–78, 1995.

Cooper AJ, Stanford IM. Electrophysiological and morphological characteristics of three subtypes of rat globus pallidus neurone in vitro. *J Physiol* 527: 291–304, 2000.

Csicsvari J, Jamieson B, Wise KD, Buzsaki G. Mechanisms of gamma oscillations in the hippocampus of the behaving rat. *Neuron* 37: 311–322, 2003.

DeLong MR. Primate models of movement disorders of basal ganglia origin. *Trends Neurosci* 13: 281–285, 1990.

Destexhe A, Rudolph M, Pare D. The high-conductance state of neocortical neurons in vivo. *Nat Rev* 4: 739–751, 2003.

Do MT, Bean BP. Subthreshold sodium currents and pacemaking of subthalamic neurons: modulation by slow inactivation. *Neuron* 39: 109–120, 2003.

Fuchs EC, Zivkovic AR, Cunningham MO, Middleton S, Lebeau FE, Bannerman DM, Rozov A, Whittington MA, Traub RD, Rawlins JN, Monyer H. Recruitment of parvalbumin-positive interneurons determines hippocampal function and associated behavior. *Neuron* 53: 591–604, 2007.

Graybiel AM, Aosaki T, Flaherty AW, Kimura M. The basal ganglia and adaptive motor control. *Science* 265: 1826–1831, 1994.

Gritti I, Henny P, Galloni F, Mainville L, Mariotti M, Jones BE. Stereological estimates of the basal forebrain cell population in the rat, including neurons containing choline acetyltransferase, glutamic acid decarboxylase or phosphate-activated glutaminase and colocalizing vesicular glutamate transporters. *Neuroscience* 143: 1051–1064, 2006.

Haines E. Point in polygon strategies. In: *Graphics Gems IV*, edited by Heckbert P. New York: Academic, 1994, p. 24–46.

Halasy K, Buhl EH, Lorinczi Z, Tamas G, Somogyi P. Synaptic target selectivity and input of GABAergic basket and bistratified interneurons in the CA1 area of the rat hippocampus. *Hippocampus* 6: 306–329, 1996.

Hallworth NE, Bevan MD. Globus pallidus neurons dynamically regulate the activity pattern of subthalamic nucleus neurons through the frequency-dependent activation of postsynaptic GABAA and GABAB receptors. *J Neurosci* 25: 6304–6315, 2005.

Hamani C, Neimat J, and Lozano AM. Deep brain stimulation for the treatment of Parkinson's disease. *J Neural Transmission* 393–399, 2006.

Hanson JE, Smith Y, Jaeger D. Sodium channels and dendritic spike initiation at excitatory synapses in globus pallidus neurons. *J Neurosci* 24: 329–340, 2004.

Hasenstaub A, Shu Y, Haider B, Kraushaar U, Duque A, McCormick DA. Inhibitory postsynaptic potentials carry synchronized frequency information in active cortical networks. *Neuron* 47: 423–435, 2005.

Hornykiewicz O. The discovery of dopamine deficiency in the parkinsonian brain. *J Neural Transmission* 9–15, 2006.

Israel Z, Bergman H. Pathophysiology of the basal ganglia and movement disorders: from animal models to human clinical applications. *Neurosci Biobehav Rev* 32: 367–377, 2008.

Kincaid AE, Zheng T, Wilson CJ. Connectivity and convergence of single corticostriatal axons. *J Neurosci* 18: 4722–4731, 1998.

Kita H, Kitai ST. The morphology of globus pallidus projection neurons in the rat: an intracellular staining study. *Brain Res* 636: 308–319, 1994.

Klausberger T, Somogyi P. Neuronal diversity and temporal dynamics: the unity of hippocampal circuit operations. *Science* 321: 53–57, 2008.

Kraushaar U, Jonas P. Efficacy and stability of quantal GABA release at a hippocampal interneuron-principal neuron synapse. *J Neurosci* 20: 5594–5607, 2000.

Levy R, Dostrovsky JO, Lang AE, Sime E, Hutchison WD, Lozano AM. Effects of apomorphine on subthalamic nucleus and globus pallidus internus neurons in patients with Parkinson's disease. *J Neurophysiol* 86: 249–260, 2001.

Levy R, Hutchison WD, Lozano AM, Dostrovsky JO. High-frequency synchronization of neuronal activity in the subthalamic nucleus of parkinsonian patients with limb tremor. *J Neurosci* 20: 7766–7775, 2000.

Loucif KC, Wilson CL, Baig R, Lacey MG, Stanford IM. Functional interconnectivity between the globus pallidus and the subthalamic nucleus in the mouse brain slice. *J Physiol* 567: 977–987, 2005.

Magill PJ, Bolam JP, Bevan MD. Dopamine regulates the impact of the cerebral cortex on the subthalamic nucleus-globus pallidus network. *Neuroscience* 106: 313–330, 2001.

Magill PJ, Bolam JP, Bevan MD. Relationship of activity in the subthalamic nucleus-globus pallidus network to cortical electroencephalogram. *J Neurosci* 20: 820–833, 2000.

Mallet N, Pogosyan A, Marton L, Bolam JP, Brown P, Magill PJ. Parkinsonian beta oscillations in the external globus pallidus and their relationship with subthalamic nucleus activity. *J Neurosci* 28: 14245–14258, 2009.

Mallet N, Pogosyan A, Sharott A, Csicsvari J, Bolam JP, Brown P, Magill PJ. Disrupted dopamine transmission and the emergence of exaggerated beta oscillations in subthalamic nucleus and cerebral cortex. *J Neurosci* 28: 4795–4806, 2008b.

Margrie TW, Brecht M, Sakmann B. In vivo, low-resistance, whole-cell recordings from neurons in the anaesthetized and awake mammalian brain. *Pfluegers* 444: 491–498, 2002.

Maurice N, Deniau JM, Glowinski J, Thierry AM. Relationships between the prefrontal cortex and the basal ganglia in the rat: physiology of the cortico-nigral circuits. *J Neurosci* 19: 4674–4681, 1999.

Miles R, Toth K, Gulyas AI, Hajos N, Freund TF. Differences between somatic and dendritic inhibition in the hippocampus. *Neuron* 16: 815–823, 1996.

Moran A, Bergman H, Israel Z, Bar-Gad I. Subthalamic nucleus functional organization revealed by parkinsonian neuronal oscillations and synchrony. *Brain* 131: 3395–3409, 2009.

Nambu A, Tokuno H, Hamada I, Kita H, Imanishi M, Akazawa T, Ikeuchi Y, Hasegawa N. Excitatory cortical inputs to pallidal neurons via the subthalamic nucleus in the monkey. *J Neurophysiol* 84: 289–300, 2000.

Nernst W. Zur kinetik der in Losung Befindlichen Korper: Theorie der Diffusion. *Z Phys Chem* 3: 613–637, 1888.

Oorschot DE. Total number of neurons in the neostriatal, pallidal, subthalamic, and substantia nigral nuclei of the rat basal ganglia: a stereological study using the cavalieri and optical disector methods. *J Comp Neurol* 366: 580–599, 1996.

Pedroarena CM, Schwarz C. Efficacy and short-term plasticity at GABAergic synapses between Purkinje and cerebellar nuclei neurons. *J Neurophysiol* 89: 704–715, 2003.

Person AL, Perkel DJ. Unitary IPSPs drive precise thalamic spiking in a circuit required for learning. *Neuron* 46: 129–140, 2005.

Pinault D. A novel single-cell staining procedure performed in vivo under electrophysiological control: morpho-functional features of juxtacellularly labeled thalamic cells and other central neurons with biocytin or Neurobiotin. *J Neurosci Methods* 65: 113–136, 1996.

Plenz D, Kital ST. A basal ganglia pacemaker formed by the subthalamic nucleus and external globus pallidus. *Nature* 400: 677–682, 1999.

Press W, Teukolsky S, Vetterling W, Flannery B. Random numbers. In: *Numerical Recipes in C: The Art of Scientific Computing* (2nd ed.). Cambridge: University Press, 1992, p. 280–282.

Raz A, Vaadia E, Bergman H. Firing patterns and correlations of spontaneous discharge of pallidal neurons in the normal and the tremulous 1-methyl-4-phenyl-1,2,3,6-tetrahydropyridine vervet model of parkinsonism. *J Neurosci* 20: 8559–8571, 2000.

Robinson HP, Kawai N. Injection of digitally synthesized synaptic conductance transients to measure the integrative properties of neurons. *J Neurosci Methods* 49: 157–165, 1993.

Sadek AR, Magill PJ, Bolam JP. A single-cell analysis of intrinsic connectivity in the rat globus pallidus. *J Neurosci* 27: 6352–6362, 2007.

Sharp AA, O'Neil MB, Abbott LF, Marder E. Dynamic clamp: computer-generated conductances in real neurons. *J Neurophysiol* 69: 992–995, 1993.

Shen KZ, Johnson SW. Presynaptic dopamine D2 and muscarine M3 receptors inhibit excitatory and inhibitory transmission to rat subthalamic neurons in vitro. *J Physiol* 525: 331–341, 2000.

Shink E, Bevan MD, Bolam JP, Smith Y. The subthalamic nucleus and the external pallidum: two tightly interconnected structures that control the output of the basal ganglia in the monkey. *Neuroscience* 73: 335–357, 1996.

Small J. Measurement of section thickness. In: *Fourth European Regional Conference on Electron Microscopy.* Rome, Italy, 609–610, 1968.

Smith Y, Bevan MD, Shink E, Bolam JP. Microcircuitry of the direct and indirect pathways of the basal ganglia. *Neuroscience* 86: 353–387, 1998.

Smith Y, Bolam JP. The output neurones and the dopaminergic neurones of the substantia nigra receive a GABA-containing input from the globus pallidus in the rat. *J Comp Neurol* 296: 47–64, 1990.

Smith Y, Bolam JP, Von Krosigk M. Topographical and synaptic organization of the GABA-containing pallidosubthalamic projection in the rat. *Eur J Neurosci* 2: 500–511, 1990.

Staley KJ, Soldo BL, Proctor WR. Ionic mechanisms of neuronal excitation by inhibitory $GABA_A$ receptors. *Science* 269: 977–981, 1995.

Tepper JM, Wilson CJ, Koos T. Feedforward and feedback inhibition in neostriatal GABAergic spiny neurons. *Brain Res Rev* 58: 272–281, 2008.

Terman D, Rubin JE, Yew AC, Wilson CJ. Activity patterns in a model for the subthalamopallidal network of the basal ganglia. *J Neurosci* 22: 2963–2976, 2002.

Urbain N, Gervasoni D, Souliere F, Lobo L, Rentero N, Windels F, Astier B, Savasta M, Fort P, Renaud B, Luppi PH, Chouvet G. Unrelated course of subthalamic nucleus and globus pallidus neuronal activities across vigilance states in the rat. *Eur J Neurosci* 12: 3361–3374, 2000.

Waters J, Helmchen F. Background synaptic activity is sparse in neocortex. *J Neurosci* 26: 8267–8277, 2006.

West MJ. Stereological methods for estimating the total number of neurons and synapses: issues of precision and bias. *Trends Neurosci* 22: 51–61, 1999.

Wichmann T, Bergman H, DeLong MR. The primate subthalamic nucleus. I. Functional properties in intact animals. *J Neurophysiol* 72: 494–506, 1994.

Zaborsky L, Pang K, Somogyi J, Nadasdy Z, Kallo I. The basal forebrain corticopetal system revisited. *Ann NY Acad Sci* 877: 339–367, 1999.

Zheng T, Wilson CJ. Corticostriatal combinatorics: the implications of corticostriatal axonal arborizations. *J Neurophysiol* 87: 1007–1017, 2002.